NANO · MICRO
small

Supporting Information

for *Small*, DOI 10.1002/smll.202308172

Enhancing Interfacial Ferromagnetism and Magnetic Anisotropy of $CaRuO_3/SrTiO_3$ Superlattices via Substrate Orientation

Wenxiao Shi, Jie Zheng, Zhe Li, Mengqin Wang, Zhaozhao Zhu, Jine Zhang, Hui Zhang, Yunzhong Chen, Fengxia Hu, Baogen Shen, Yuansha Chen and Jirong Sun**

Supporting Information for

Enhancing interfacial ferromagnetism and magnetic anisotropy of $CaRuO_3/SrTiO_3$ superlattices via substrate orientation

Wenxiao Shi, Jie Zheng, Zhe Li, Mengqin Wang, Zhaozhao Zhu, Jine Zhang, Hui Zhang, Yunzhong Chen, Fengxia Hu, Baogen Shen, Yuansha Chen* and Jirong Sun*

*Corresponding author. Email: yschen@iphy.ac.cn (Y.S.C); jrsun@iphy.ac.cn (J.R.S)

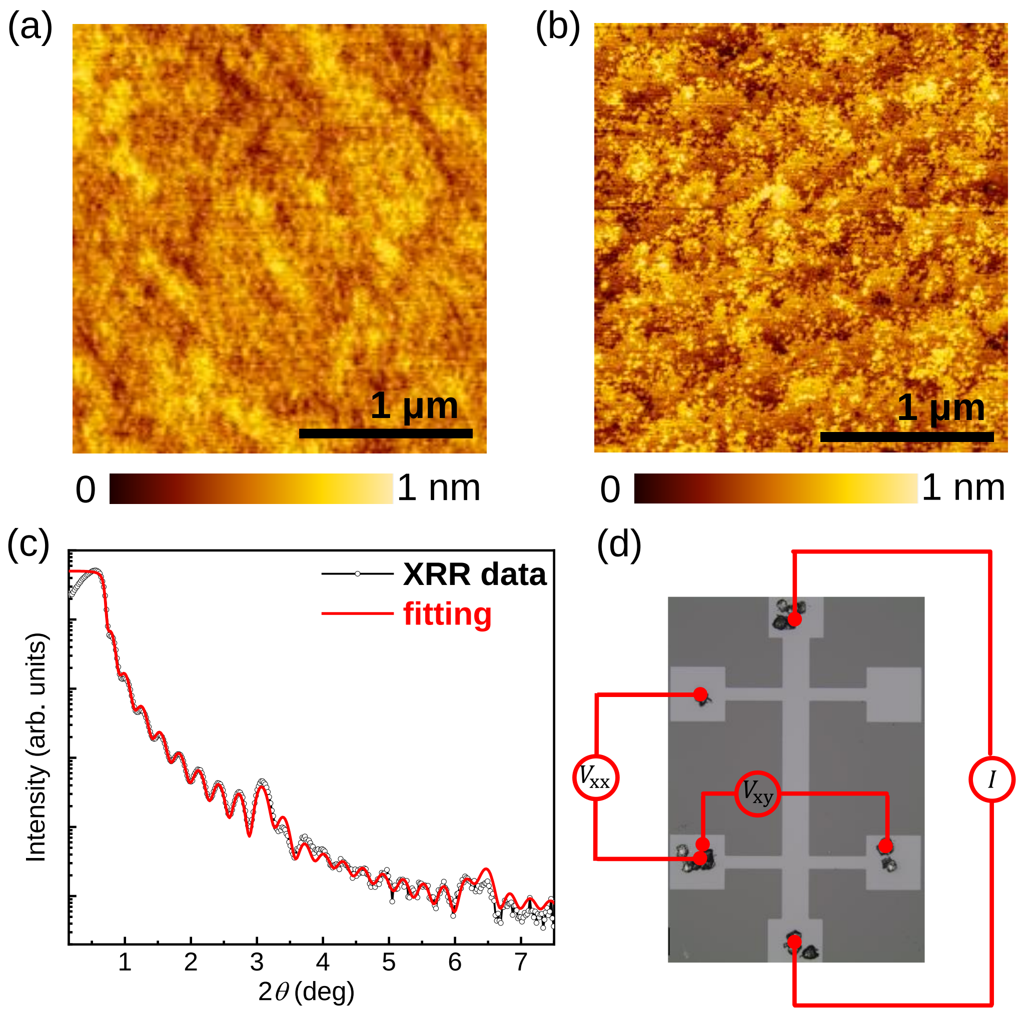

Figure S1. (**a**) AFM topography of (111)-LSAT substrate after the annealing in oxygen pressure of 1 atm at 900 °C for 2 hours. The substrate surface is atomically-flat, with a root-mean-squared roughness of ~1.1 Å. (**b**) AFM topography of $(CRO_{10}/STO_3)_{10}$ SL deposited on LSAT (111) surface, with a root-mean-squared roughness of ~1.5 Å. Image size is 2.5 μm × 2.5 μm. (**c**) XRR of the $(CRO_{10}/STO_3)_{10}$ SL grown on the (111)-oriented LSAT substrate. Good agreement between fitting curve (red) and experimental curve (black) is clearly demonstrated. The simulation curve is realized by the commercial software of DIFFRAC^{plus} LEPTOS 7. The deduced thickness of CRO and STO layers is consistent with the targeted structure. (**d**) Optical image of the Hall bar device for electric measurements. The dimension of the Hall bar is 200 μm in width and 1300 μm in length (the distance between the two voltage electrodes V_{xx}).

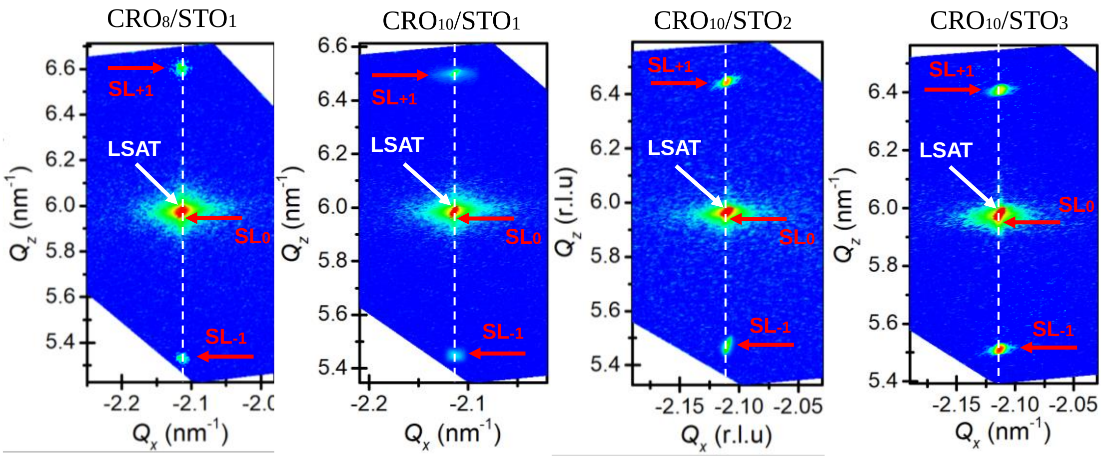

Figure S2. RSM around (112) reflection for the $(CRO_8/STO_1)_{10}$, $(CRO_{10}/STO_1)_{10}$, $(CRO_{10}/STO_2)_{10}$ and $(CRO_{10}/STO_3)_{10}$ SLs. The satellite peaks are detected for these SLs, which also vertically align with the diffraction spot of substrate. It suggests that the SLs investigated in this manuscript are all fully strained to the LSAT substrate, suffering from the same in-plane strain.

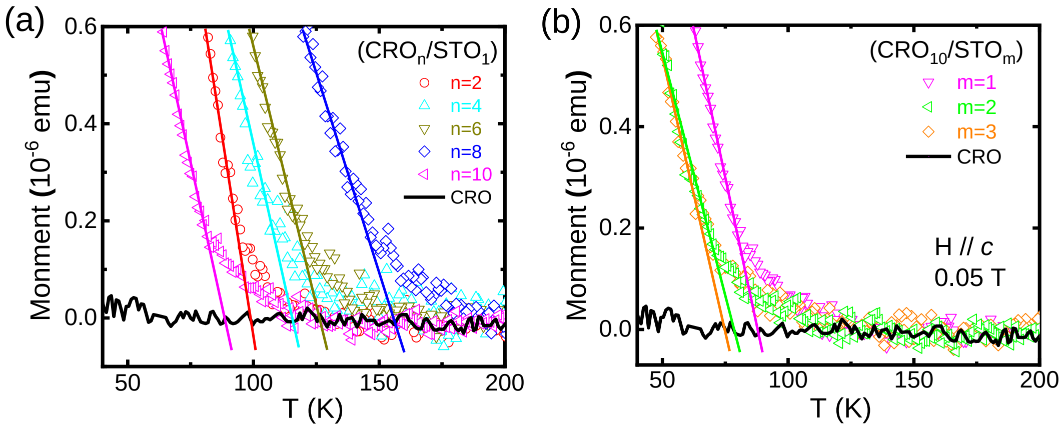

Figure S3. Enlarged M-T curves for **(a)** $(CRO_n/STO_1)_{10}$ and **(b)** $(CRO_{10}/STO_m)_{10}$ SLs on (111)-oriented LSAT substrate, measured with an out-of-plane field of 0.05 T in field-cooling mode. T_C is deduced for each CRO/STO SL, using the zero-crossing temperature of the tangent line.

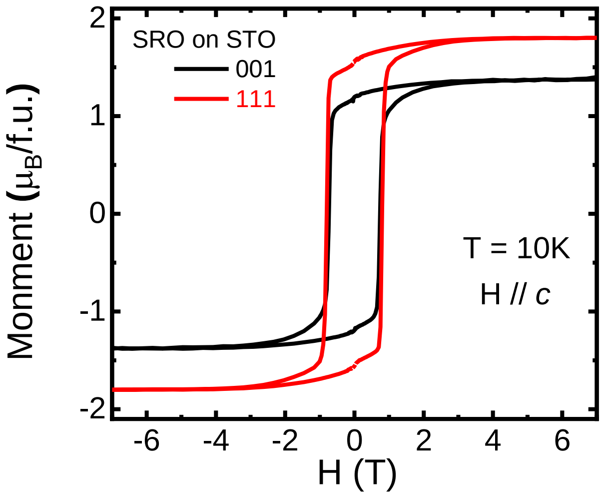

Figure S4. Magnetic moment as a function of applied magnetic field (*H*) at 10 K for the $SrRuO_3$ films (with the same 30 nm thickness) deposited on (001) and (111)-oriented STO substrates. The saturated moment (*Ms*) increase from the 1.4 μB/f.u. of (001)-oriented $SrRuO_3$ to the 1.8 μB/f.u. of (111)-oriented $SrRuO_3$ film.

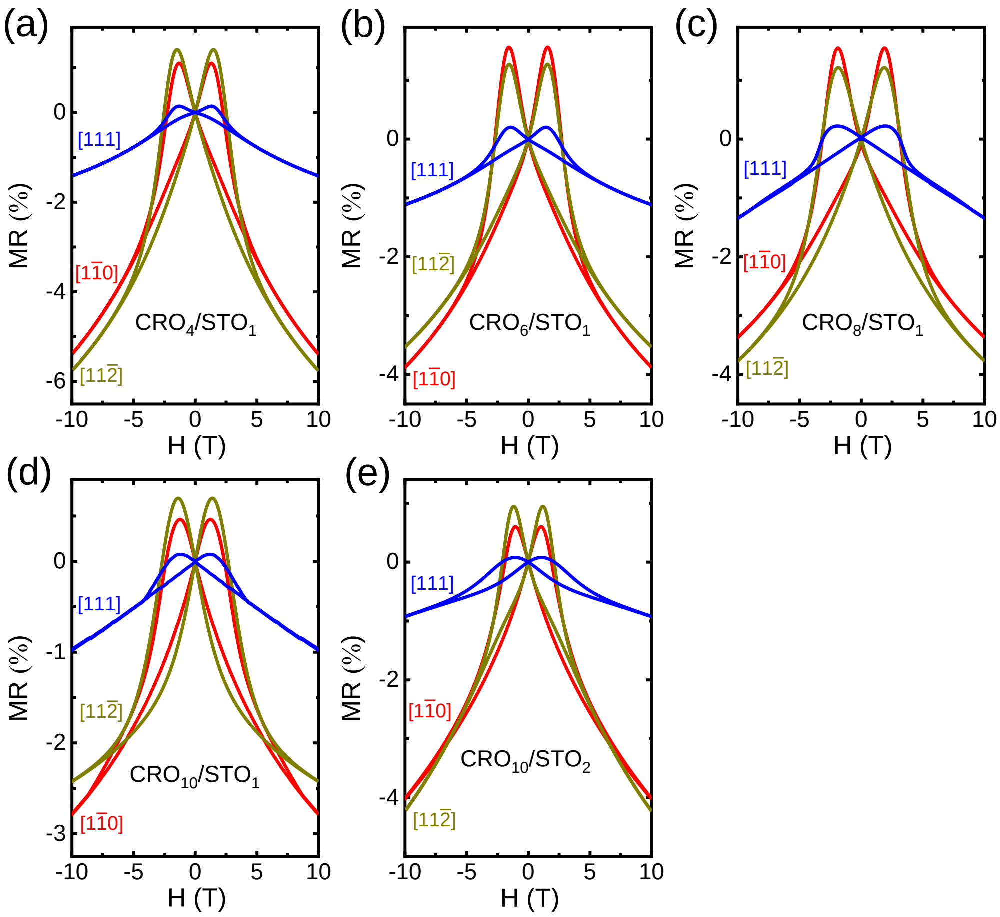

Figure S5. (**a**) MR at T = 2 K for $(CRO_4/STO_1)_{10}$, (**b**) $(CRO_6/STO_1)_{10}$, (**c**) $(CRO_8/STO_1)_{10}$, (**d**) $(CRO_{10}/STO_1)_{10}$ and (**e**) $(CRO_{10}/STO_2)_{10}$ SLs with the magnetic field applied parallel to $[1\bar{1}0]$, $[11\bar{2}]$ and $[111]$ directions.

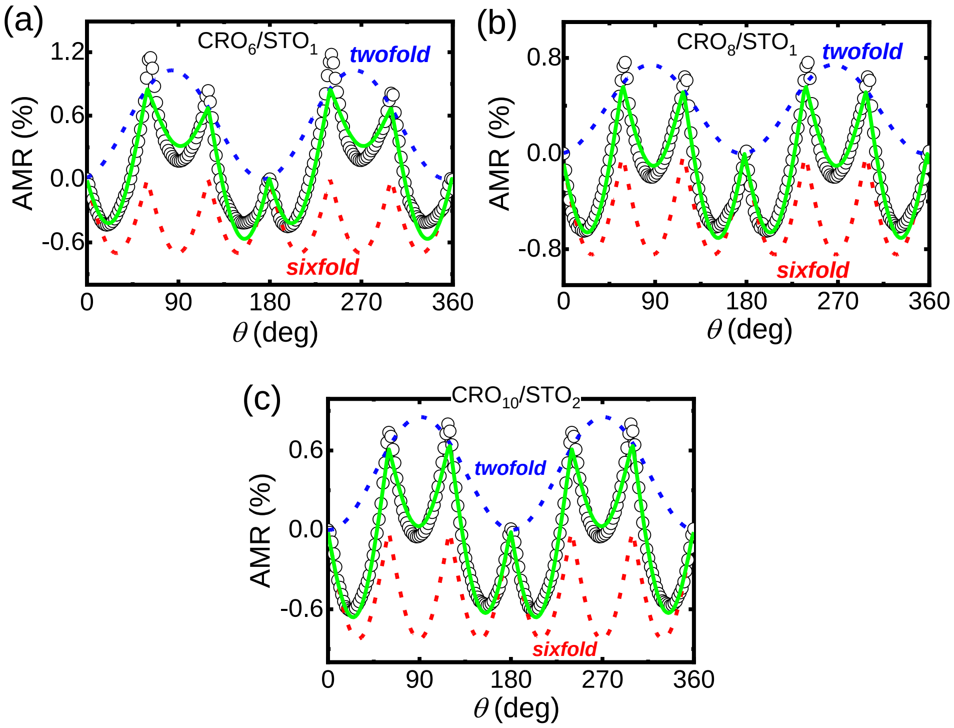

Figure S6. (a)-(c) Angle dependence of the AMR measured at 2 K and 10 T for the $(CRO_6/STO_1)_{10}$ SL (a), $(CRO_8/STO_1)_{10}$ SL (b) and $(CRO_{10}/STO_2)_{10}$ SL (c) on (111)-oriented LSAT substrate. The experimental data (black symbols) can be well described by $\mathrm{AMR}(\theta) = c_2 \times \cos(2\theta - \omega_2) + c_6 \times \cos\left[6 \times \left(\theta - \frac{\sin(6\theta)}{4H/H_a^{in} + 6 \times \cos(6\theta)}\right) - \omega_6\right]$ with two contributions of sixfold (red curve) and twofold (blue curve) symmetries, where c_2 and c_6 are the amplitudes of AMR contributions with two-fold and six-fold symmetries. Green lines are the results of curve-fitting. Satisfactory agreement with experiment results is obtained adopting suitable fitting parameters.

Section S1. Non-cosine square angular-dependent magnetoresistance of the honeycomb lattice structure

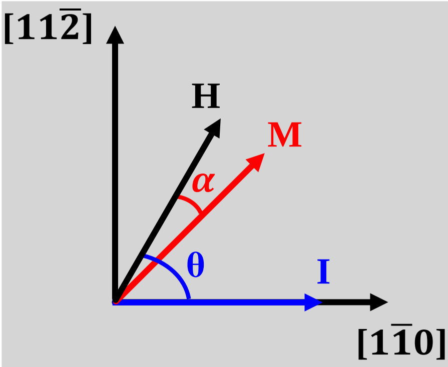

To describe the deviation of $\boldsymbol{M_s}$ from $\boldsymbol{H}$, we considered the Zeeman energy and the honeycomb lattice magnetocrystalline anisotropy energy characterized by a constant K_{in}, the in-plane free energy density is written as: [1-2]

$$F_{in} = -\mu_0 M_S H \cos\alpha + \frac{1}{6} K_{in} \sin^2 3(\theta - \alpha) \tag{1}$$

where μ_0 is the permeability of vacuum and M_S is saturation magnetization. The equilibrium direction of $\boldsymbol{M_S}$ is determined by $\partial F_{in}/\partial\alpha = 0$, that is

$$h \sin\alpha - \frac{1}{4} sin\, 6(\theta - \alpha) = 0 \tag{2}$$

where the reduced field $h = H/H_a^{in}$, the in-plane anisotropic filed $H_a^{in} = 2K_{in}/\mu_0 M_S$.

Then, we used Taylor's series for Eq. (2) at $\alpha = 0$, and obtained a similar result as follow:

$$\alpha = \frac{\sin(6\theta)}{4H/H_a^{in} + 6\times\cos(6\theta)} \tag{3}$$

Therefore, the in-plane AMR formula under the small-angle approximation is written as:[3]

$$\mathrm{AMR} = c_2 \times \cos(2\theta - \omega_2) + c_6 \times \cos\left[6 \times \left(\theta - \frac{\sin(6\theta)}{4H/H_a^{in} + 6\times\cos(6\theta)}\right) - \omega_6\right] \tag{4}$$

References

[1] Y. Miao, X. Chen, S. Yang, K. Zheng, Z. Lian, Y. Wang, P. Wang, C. Gao, D. Z. Yang, D. S. Xue, *J. Magn. Magn. Mater.* **2020,** *512*, 167013.

[2] Y. Miao, D. Yang, L. Jia, X. Li, S. Yang, C. Gao, D. Xue, *Appl. Phys. Lett.* **2021,** *118*, 042404.

[3] P. K. Rout, I. Agireen, E. Maniv, M. Goldstein, Y. Dagan, *Phys. Rev. B* **2017,** *95*, 241107(R).